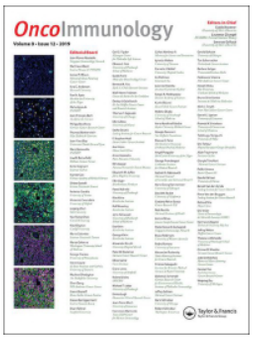

OncoImmunology

ISSN: (Print) (Online) Journal homepage: https://www.tandfonline.com/loi/koni20

Phenotypic characterization of spatial immune infiltration niches in non-small cell lung cancer

Anna Sandström Gerdtsson, Mattis Knulst, Johan Botling, Artur Mezheyeuski, Patrick Micke & Sara Ek

To cite this article: Anna Sandström Gerdtsson, Mattis Knulst, Johan Botling, Artur Mezheyeuski, Patrick Micke & Sara Ek (2023) Phenotypic characterization of spatial immune infiltration niches in non-small cell lung cancer, OncoImmunology, 12:1, 2206725, DOI: 10.1080/2162402X.2023.2206725

To link to this article: https://doi.org/10.1080/2162402X.2023.2206725

ONCOIMMUNOLOGY
2023, VOL. 12, NO. 1, 2206725
https://doi.org/10.1080/2162402X.2023.2206725

Taylor & Francis
Taylor & Francis Group

ORIGINAL RESEARCH

OPEN ACCESS Check for updates

Phenotypic characterization of spatial immune infiltration niches in non-small cell lung cancer

Anna Sandström Gerdtsson[a], Mattis Knulst[a], Johan Botling[b], Artur Mezheyeuski[b,c], Patrick Micke[b#], and Sara Ek[a#]

[a]Department of Immunotechnology, CREATE Health, Lund University, Lund, Sweden; [b]Department of Immunology, Genetics and Pathology, Uppsala University, Uppsala, Sweden; [c]Molecular Oncology Group, Vall d'Hebron Institute of Oncology, Barcelona, Spain

ABSTRACT

The immune microenvironment of non-small cell lung cancer (NSCLC) is heterogeneous, which impedes the prediction of response to immune checkpoint inhibitors. We have mapped the expression of 49 proteins to spatial immune niches in 33 NSCLC tumors and report key differences in phenotype and function associated with the spatial context of immune infiltration. Tumor-infiltrating leukocytes (TIL), identified in 42% of tumors, had a similar proportion of lymphocyte antigens compared to stromal leukocytes (SL) but displayed significantly higher levels of functional, mainly immune suppressive, markers including PD-L1, PD-L2, CTLA-4, B7-H3, OX40L, and IDO1. In contrast, SL expressed higher levels of the targetable T-cell activation marker CD27, which increased with a longer distance to the tumor. Correlation analysis confirmed that metabolic-driven immune regulatory mechanisms, including ARG1 and IDO1, are present in the TIL. Tertiary lymphoid structures (TLS) were identified in 30% of patients. They displayed less variation in the expression profile and with significantly higher levels of pan lymphocyte and activation markers, dendritic cells, and antigen presentation compared to other immune niches. TLS also had higher CTLA-4 expression than non-structured SL, which may indicate immune dysfunction. Neither the presence of TIL nor TLS was associated with improved clinical outcomes. The apparent discrimination in functional profiles of distinct immune niches, independent of the overall level of leukocytes, illustrates the importance of spatial profiling to deconvolute how the immune microenvironment can dictate a therapeutic response and to identify biomarkers in the context of immunomodulatory treatment.

ARTICLE HISTORY
Received 19 January 2023
Revised 3 April 2023
Accepted 21 April 2023

KEYWORDS
NSCLC; immune infiltration; tertiary lymphoid structures; tumor-infiltrating leukocytes; spatial omics

Introduction

Non-small cell lung cancer (NSCLC) is the leading cause of cancer-related deaths, with a 5-year survival rate of 15–20%[1]. Treatment with small synthetic inhibitors targeting mutated receptor kinases, like EGFR or ALK, results in improved survival in a minority of lung cancer patients[2,3]. For lung cancer patients with tumors without mutations in cancer driver genes, the introduction of immune checkpoint inhibitors (ICIs), alone or combined with chemotherapy treatment, leads to long-term responses in a small subset of patients[4,5]. However, the majority of patients do not substantially respond to these treatment options, and a reliable selection of individuals who benefit most is of high clinical need. The currently applied assays, measuring PD-L1 expression on tumor cells, have limited performance for predicting response to treatment. Thus, improved stratification of patients is still warranted. Furthermore, major efforts to identify other immune targets are ongoing to increase the spectrum of patients that respond to immune-modulating agents.

The efficacy of ICI depends on the presence of tumor-infiltrating immune cells as well as levels of T-cell exhaustion, immune suppression, and angiogenesis[6,7]. The spatial organization of immune cells within the histological structure of the tumor and proximity of cells have more recently been identified as crucial factors for anti-cancer immunity[8,9]. The NSCLC tumor immune microenvironment (TIME) exhibits vast inter- and intra-tumor heterogeneity[10], motivating comprehensive characterization to optimally inform clinical decision-making. The advent of high-plex spatial omics technologies is currently revolutionizing the field of digital pathology and offers an opportunity for detailed mapping of individual tumors[11]. Here, we have applied GeoMx Digital Spatial Profiling (DSP) to deconvolute phenotypic and functional composition of distinct immune infiltration niches in NSCLC, to identify targetable markers and TIME signatures reflecting spatial organization of immune infiltrates.

Material and methods

Patient cohort and TMA

A tissue microarray (TMA) of surgically resected NSCLC tissue, with two 1-mm-diameter cores per tumor, had been previously constructed from tissue collected between 2006 and 2010 at the Uppsala University Hospital[12] (Uppsala Ethical

CONTACT Anna Sandström Gerdtsson anna.sandstrom_gerdtsson@immun.lth.se Department of Immunotechnology, CREATE Health, Lund University, Medicon Village 406, Scheelevägen 8, Lund 223 87, Sweden
[#]Shared authorship

Supplemental data for this article can be accessed online at https://doi.org/10.1080/2162402X.2023.2206725

Table 1. Clinicopathological information for the NSCLC cohort.

	Patients, $n = 33$
Age	
Median	69
Min	56
Max	83
Gender	
Female	15
Male	18
Histology	
Adenocarcinoma	17
Squamous cell carcinoma	15
Stage	
IA	9
IB	6
IIA	4
IIB	5
IIIA	9
Lymph node stage	
N0	23
N1	4
N2	6
Smoking	
Current	12
Former	19
Never	2
Overall survival (years)	
Median	6.35
Min	0.02
Max	10.02
Progression-free survival (years)	
Median	3.89
Min	0.42
Max	7.23
TLS-pos TMA cores	
Yes	10
No	23
PD-L1-pos IHC (10% cutoff)	
Yes	14
No	19

Review Board, reference 2012/532). Tumor cores from 58 patients were included in the TMA. Tumors were excluded due to patients having received neoadjuvant treatment ($n = 5$), being outside the GeoMx scan area ($n = 12$), or insufficient content of intact cells ($n = 8$), due to, e.g., poor quality tissue, low tumor content, large necrotic areas, or low immune content. Clinical data from 33 patients with evaluable tissue that were used for DSP analysis are provided in Table 1. Data from RNA sequencing, mutational status for 82 genes, and mutational load, as well as immunohistochemistry (IHC) data from the same TMA, were available from previous studies[13,14]. Genes with mutations in at least 6/33 patients (KRAS, $n = 8$; NF1, $n = 6$; STK11, $n = 7$; TP53, $n = 20$; MUC16, $n = 14$, KMT2C, $n = 6$; KMT2D, $n = 9$; CSMD3, $n = 15$; and LRP1B, $n = 6$) were checked for effect on immune biomarker expression by comparing mutated (any mutation) to wild type (wt).

GeoMx digital spatial profiling

A TMA slide was stained with an immunofluorescence (IF) morphology panel of Pan-CK, CD45, and Syto13 and 49 oligo-conjugated DSP antibodies (Table 2), according to the GeoMx protein profiling protocol (Nanostring)[15]. The slide was scanned in the DSP instrument (Figure 1A) and ROI selection was guided by the 3-color composite IF image. ROIs were selected based on spatial localization and structure, by ocular review and consensus among three analysts (PM, SE, and ASG), and classified as either tumor-infiltrating leukocytes (TIL) (dispersed among tumor cells), stromal leukocytes (SL) (separated from tumor cells), or tertiary lymphoid structures (TLS) (dense stromal leukocyte compartments of high CD45 intensity) (Figure 1B,D). In addition, ROIs were manually and visually scored on a 1–4 scale based on decreasing distance to the tumor, with 1 = no immune-tumor spatial contact, 2 = distinct clusters of immune cells located close to the tumor margin, 3 = clusters of immune

Table 2. Digital spatial profiling antibody panel.

Protein panel for TIME profiling				
4-1BB	CD25	CD56	GITR	PD-1
ARG1	CD27	CD66b	GZMB	PD-L1
B7-H3	CD3	CD68	HLA-DR	PD-L2
B2M	CD34	CD8	ICOS	SMA
CD11c	CD4	CD80	IDO1	STING
CD127	CD40	CTLA4	Ki-67	Tim-3
CD14	CD44	FAP-a	LAG3	VISTA
CD163	CD45	Fibronectin	OX40L	
CD20	CD45RO	FoxP3	Pan-CK	
Controls				
House-keeper proteins		Histone H3	S6	GAPDH
Isotype controls		Ms IgG1	Ms IgG2a	Rb IgG

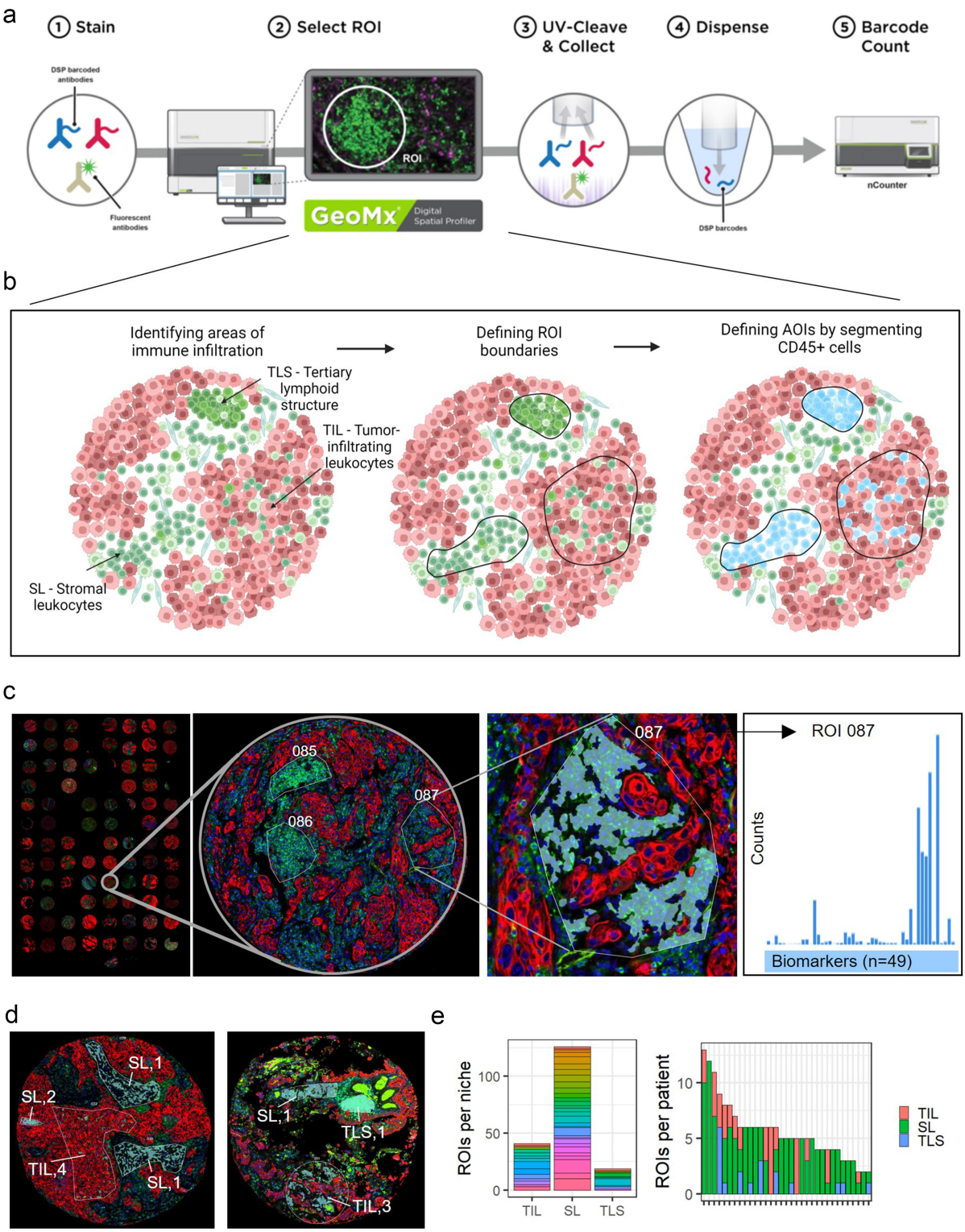

Figure 1. Study design and region of interest (ROI) selection, classification, and distribution across patients. (A) Overview of the GeoMx Digital Spatial Profiling (DSP) workflow. (B) Schematic overview of spatially distinct areas of immune infiltration in NSCLC, definition of ROIs, and segmentation into areas of illumination (AOIs) to select CD45+ cells for multiplex protein characterization. Importantly, one AOI could consist of several non-overlapping segments within the same ROI. (C) ROIs were selected from a TMA with duplicate tissue cores, visualized by 3-color immunofluorescence (IF) (blue = Syto13, red = Pan-CK, green = CD45), with multiple ROIs selected per tumor. Within each ROI, an AOI was defined by segmenting CD45+, Syto13+, and Pan-CK- immune cells. Antibody binding events of 49 proteins were quantified within each AOI. (D) ROIs were classified based on spatial localization as stromal leukocytes (SL), tumor-infiltrating leukocytes (TIL), or tertiary lymphoid structures (TLS), as well as by distance to tumor margin. Numbers correspond to distance scoring on a 1–4 scale where 1 is furthest from the tumor margin and 4 is closest. (E) Frequency of TIL, SL, and TLS ROIs, colored by patient (left), and per patient (right). Each bar represents one patient, and ROIs are colored by spatial phenotype.

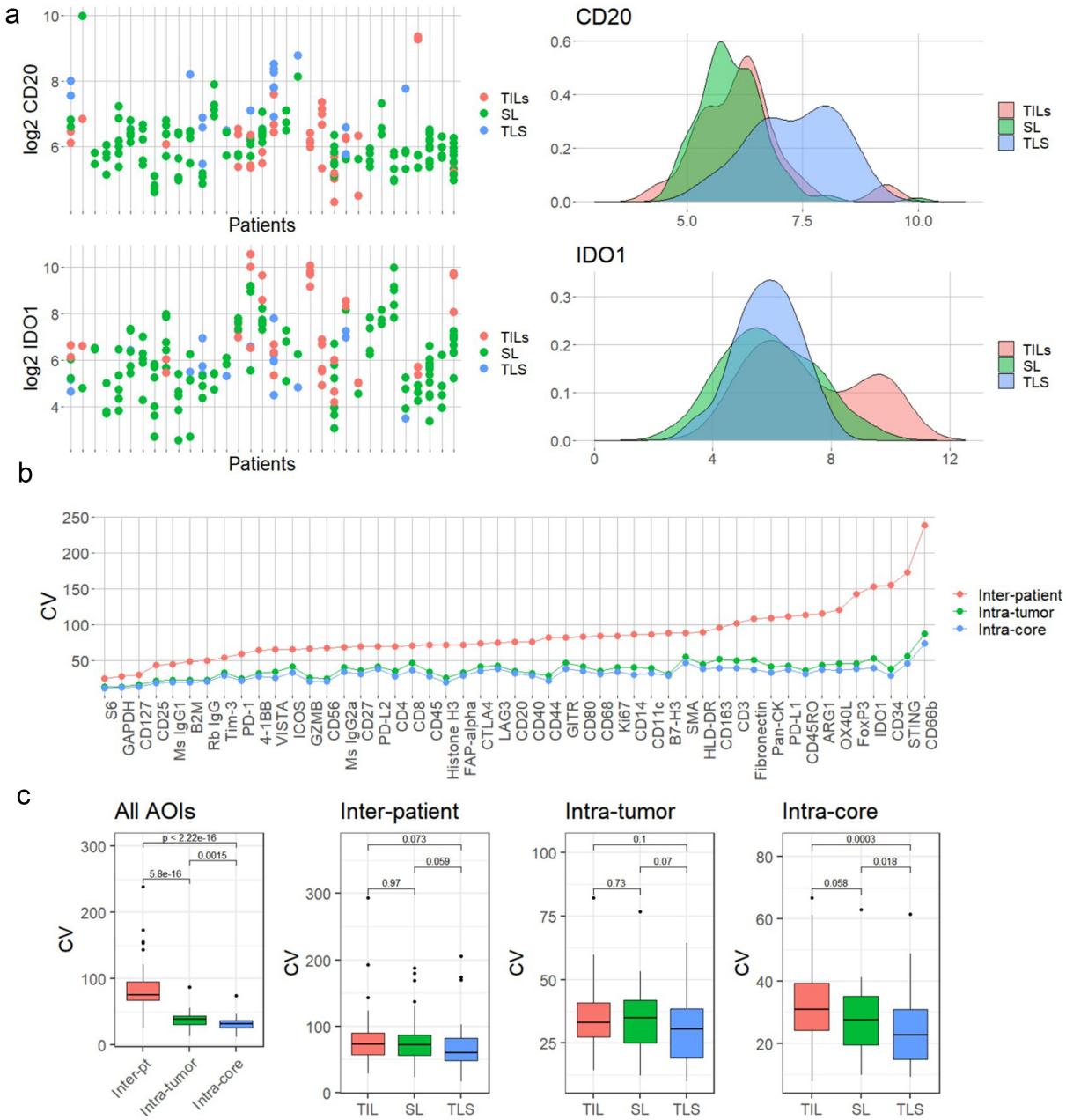

Figure 2. Tumor immune microenvironment (TIME) heterogeneity across patients and spatial immune niches. (A) Patient dependency of biomarker baseline level as shown for IDO1 (high in TIL) and CD20 (high in TLS), with data plotted per patient (left panels) and density plots with log2 data value on the x axis and the kernel density estimate on the y-axis (right panels), colored by type of spatial CD45 niche (TIL, SL, and TLS). (B) Variation per biomarker shown as inter-patient CV (measured across all AOIs), intra-tumor average CV (all AOIs per patient), and intra-core average CV (AOIs from the same tumor core). (C) Inter-patient, intra-tumor, and intra-core CVs across all biomarkers, shown for all AOIs (left panel), and per spatial immune niche, respectively.

cells interspersed in tumor compartments, and 4 = immune cells highly dispersed among and in direct contact with cancer cells (Figure 1D). In each ROI, immune cells (CD45+, Syto13+, and Pan-CK-) were marked and constituted the Area of Illumination (AOIs) collected from the specific ROI (Figure 1B-C). Oligo identifiers were released by sequentially exposing each AOI to UV illumination and collected in separate wells of a microtiter plate. The TMA was analyzed in two separate scans, with a total of 183 AOIs being collected. Oligo identifiers were hybridized into color coded barcodes and quantified using nCounter (Nanostring).

Data processing and analysis

Normalization strategies were evaluated by assessing the factors (positive and negative control antibodies, AOI area, and AOI nuclei count) that most efficiently could compensate for systematic differences in signal strengths between spatial niches (Supplementary Figure S1), which resulted in that scaling antibody signals to the geometric mean of housekeeper (HK) proteins GAPDH and S6 for each AOI was adopted. Biomarker variation was assessed by the log2 signal-to-background ratio, calculated as the relative signal to the geometric mean of three isotype controls (Mouse

IgG1, Mouse IgG2a, and Rabbit IgG) per AOI (Figure 2B). Biomarkers with negative log signal-to-background median values were flagged but not excluded from the analysis as all biomarkers showed positive signals in subsets of AOIs. Inter-patient, inter-core, and intra-core variations were assessed by calculating the coefficient of variation (CV) as the standard deviation over the mean for each biomarker (Figures 2C,D). Linear mixed models (LMM) with Patient ID as random effect were applied to identify differentially expressed proteins between categorical variables, including spatial phenotypes and mutational status, or associated to ordinal scale variables, including distance to tumor (1-4), tumor stage (1 = 1A, 2 = 1B, 3 = 2A, 4 = 2B, 5 = 3A), and lymph node stage (0 = N0, 1 = N1, 2 = N2), using the lmer function of the lmerTest package for R. Wilcoxon signed-ranked tests were applied for intra-patient pairwise analysis based on tumors from which at least two AOIs of different spatial niches had been collected. Correlation between biomarkers was assessed using Pearson correlation test. Association of survival was assessed using clustered univariate Cox regression with Patient ID as the clustering parameter, using the lifelines package for python. The survminer package for R was used for Kaplan–Meier analysis, with the optimal threshold for categorization identified using Maximally Selected Rank Statistics in R.

Results

Study overview and data quality control

A total of 183 ROIs were selected in spatially distinct immune areas, annotated as SL, TIL, or TLS (Figures 1A-E). TLS were located in stroma but classified separately from SL based on the distinct morphology of dense, CD45-high immune clusters. Examples of ROIs are shown in Figure 1D. In each selected ROI, leukocytes (CD45+, Syto13+, and Pan-CK- cells) were selected and constituted the AOI, from which signals were captured and analyzed (Figures 1B,C). The number of AOIs collected per spatial niche (SL, TIL, or TLS) was 126 SL from 30 patients, 40 TIL from 15 patients, and 19 TLS from 10 patients (Figure 1E). No variation was observed between the two scan batches (Supplementary Figure S1A). The discrepancy in background signal is related to variation in the nuclear count and AOI size, where in general TIL had the lowest and TLS had the highest nuclei count (Supplementary Figure S1B), was neutralized through scaling with HK proteins GAPDH and S6 (Supplementary Figure S1C). In order to assess the limit of detection and dynamic range of biomarker signals, based on a collection of different number of cells, a separate dataset of 18 ROIs was created (Supplementary Figure S2A). It was observed that both low (isotype control) and high (Histone H3) abundant proteins could be measured from as few as five cells, without significant differences in quantification of individual proteins compared to 50-fold number of cells (Supplementary Figure S2B-C). Thus, we conclude that the methodology produces robust protein signals over a wide range of cell numbers even below the 20 cells recommended in DSP protocols.

TIME heterogeneity across tumors and spatial regions

Baseline levels of individual biomarkers varied significantly across tumors, demonstrating a marked inter-tumor heterogeneity, regardless of spatial niche (Figure 2). Accordingly, several proteins displayed a non-normal distribution, attributed to the fact that multiple AOIs had been collected per patient (Figure 2A, Supplementary Figure S3). An ~8-fold log2 difference in median signal-to-background values between antigens with low and high expression was seen (Supplementary Figure S4). The highest variation across AOIs was seen for CD66b (granulocytes), followed by STING, CD34, IDO1, FoxP3, OX40L, and ARG1 (Figure 2B), with significantly higher inter-patient than intra-core variation ($p = 5.8e\text{-}16$, Figure 2C). Although the limited tissue cores included in a TMA may not present the full heterogeneity of a tumor, the intra-patient variation was only marginally higher than intra-core variation (Figure 2C), indicating that the select ROIs were representatively capturing immune infiltration across a tumor. Albeit only significant for intra-core CVs, there was a trend of lower variation in TLS compared to SL and TIL (Figure 2C). Concordantly, absolute correlation coefficients were significantly higher in TLS compared to SL and TIL ($p < 2e\text{-}16$) (Supplementary Figure S5), demonstrating that, compared to other spatial immune niches, TLS display a more homogenous protein composition across NSCLC tumors. Higher homogeneity may in part be an effect of absent signal contribution from immune-neighboring cells (e.g., tumor or stroma cells) to the distinct TLS regions.

Protein profiles of distinct spatial immune niches across tumors

The overall levels of lymphocyte phenotypic markers (e.g., CD45, CD3, CD4, CD8, and CD20) did not differ between TIL and SL. However, functional markers, as well as myeloid markers, differed significantly between these two compartments (Figure 3A). TIL had higher expression of PD-L1, B7-H3, CTLA4, OX40 L, IDO1, CD68, PD-L2, FoxP3, CD11c, CD40, and Ki-67, demonstrating an actively suppressed immune environment and the presence of ICI targets in infiltrated tumors. In contrast, SL had higher expression of the immune checkpoints CD27 and VISTA, with a background expression of fibroblast activation markers SMA and Fibronectin. Pan-CK was the most significantly differentially expressed protein due to the fact that TIL has a larger area of cell-to-cell contact with tumor cells expressing Pan-CK. Thus, background levels of highly abundant proteins in neighboring cells were also detected.

Immune compartments manifested as dense, stromal clusters of CD45-bright cells annotated as TLS were compared to unstructured stromal immune infiltration (SL). TLS were higher in CD20, CD45, CD3, HLA-DR, beta-2-microglobulin, CD11c, CTLA-4, CD40, ICOS, and Ki-67, denoting aggregates of antigen presentation with active and proliferating B- and T lymphocytes (Figure 3A). Moreover, TLS were lower in SMA, fibronectin, and VISTA compared to SL and lower in ARG1 and CD66b compared to both TIL and SL, confirming that TLS have low presence of myeloid and stromal cells in relation to other spatial immune niches.

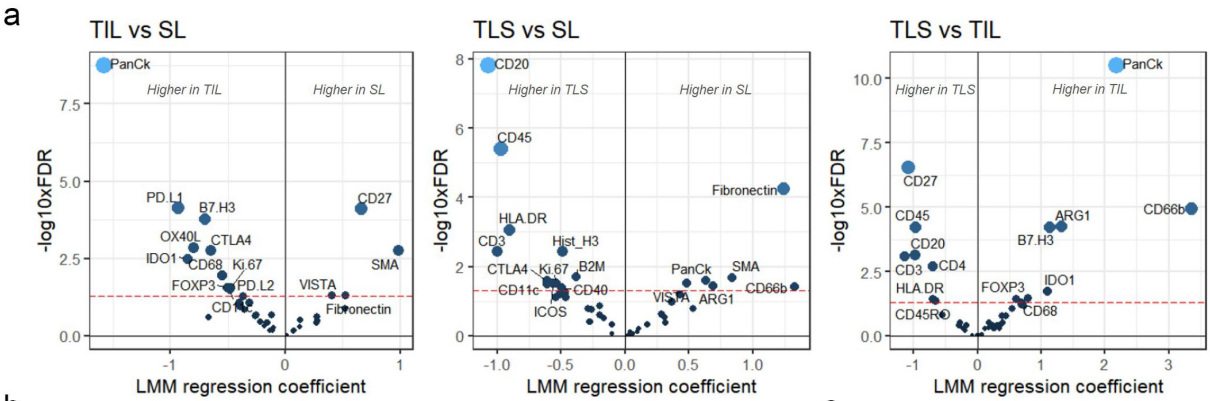

b

TIL vs SL

paired Wilcoxon test, 10 tumors

Biomarker	*p-value*	*log2 FC*
CD27	0.010	-0.31
OX40L	0.010	0.73
B7-H3	0.014	0.81
IDO1	0.037	0.76

TLS vs SL

paired Wilcoxon test, 9 tumors

Biomarker	*p-value*	*log2 FC*
CD20	0.004	1.03
CD45	0.004	0.88
CD245RO	0.004	0.28
ARG1	0.004	-0.39
Hist-H3	0.004	0.40
CD66b	0.008	-1.45
B2M	0.008	0.34
HLA-DR	0.012	0.78
CD3	0.012	0.67
Fibronectin	0.012	-0.58
CTLA4	0.027	0.53
SMA	0.027	-0.46

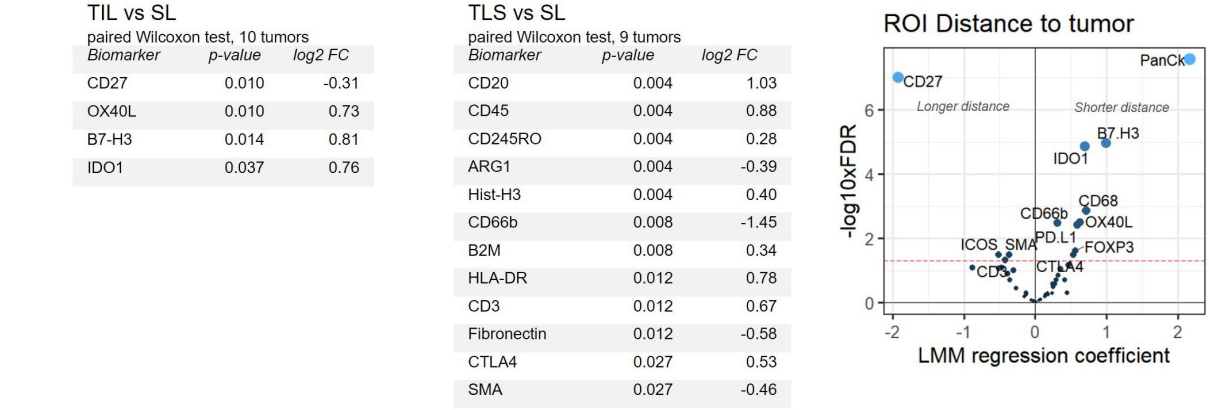

Figure 3. Phenotypic profiling of spatial immune niches. (A) Differential protein expression identified by Linear Mixed Models (LMM) with patient as random effect for TIL vs. SL (left), TLS vs. SL (middle), and TLS vs. TIL (right). -log10 FDR (false discovery rate) was plotted against LMM regression coefficient, with FDR = 0.05 marked by dotted red line. In each comparison, negative regression coefficients denote higher expression in TIL vs. SL; TLS vs. SL; and TLS vs. TIL, and vice versa. (B) Wilcoxon signed-ranked test p-values from paired analysis of tumors from which more than one spatial niche had been sampled. P-values and log2 fold changes for TIL vs. SL (left) and TLS vs. SL (right). Biomarkers with significant p-values are listed. (C) LMM regression on ordinal scale with patient as random effect and distance to tumor as outcome, with -log10 FDR plotted against LMM regression coefficient. Positive regression coefficient corresponds to shorter distance to tumor and vice versa. FDR = 0.05 is marked by dotted red line. (D) Schematic summary of protein profiles identified for distinct spatial immune niches in NSCLC.

Several of the significant biomarkers in the linear mixed models were also identified as differentially expressed through per-patient, non-parametric paired comparisons of TIL vs. SL, and TLS vs. SL, based on a limited set of tumors from which more than one type of spatial niche had been sampled (Figure 3B). A subset of proteins, including Pan-CK ($p = 0.11$), PD-L1 ($p = 0.13$), and CD68 ($p = 0.13$) in TIL vs. SL, did not reach significance in the pairwise test, likely due to the low number of patients included and the fact that certain markers may be driven by few patients with high expression in distinct immune niches.

Immune phenotypes related to distance to tumor

Regression with ROI distance to tumor as fixed effect and patient as random effect also showed an increased immune suppressive environment with closer tumor vicinity. Expression of B7-H3, IDO1, CD68, OX40L, CD66b, PD-L1, FoxP3, and CTLA4 was significantly associated to shorter tumor immune distance (Figure 3C). As noted above, the increased expression of Pan-CK, PD-L1, IDO1, and Ki-67 with decreasing distance to the tumor may be attributed to background signals from adjacent

tumor cells rather than leukocyte-specific biomarker signals. Longer distance to the tumor was mainly associated with the immune activation marker CD27, which did not differ between SL and TLS, but was significantly higher in both compared to TIL. In addition, when excluding TLS, CD27 remained significantly associated with a longer distance to the tumor (Supplementary Figure 6), demonstrating higher overall expression in stromal immune regions located further away from the tumor cells. In general, immune checkpoints were significantly higher in TIL, with the exception of CD27 and VISTA (Figure 3A).

In summary, we show that TLS are high in lymphocyte phenotypic and activation-related proteins, antigen presentation, and proliferation markers, and the immune checkpoint CTLA-4 (Figure 3D). In contrast, non-structured stromal immune niches revealed a more heterogeneous lymphocytic repertoire and higher levels of fibroblast activation, and high CD27 expression which increases with distance to tumor. Targetable immune checkpoints were primarily expressed in the tumor-infiltrating immune compartments in direct contact with tumor cells. CD68+ macrophages as well as FoxP3+ immune regulatory lymphocytes were also enriched in TIL, although it should be noted that FoxP3 was overall low, and thus, its differential expression should be interpreted with care. Levels of CD66b+ granulocytes did not differ between infiltrating and stromal immune niches but were higher in both compared to TLS.

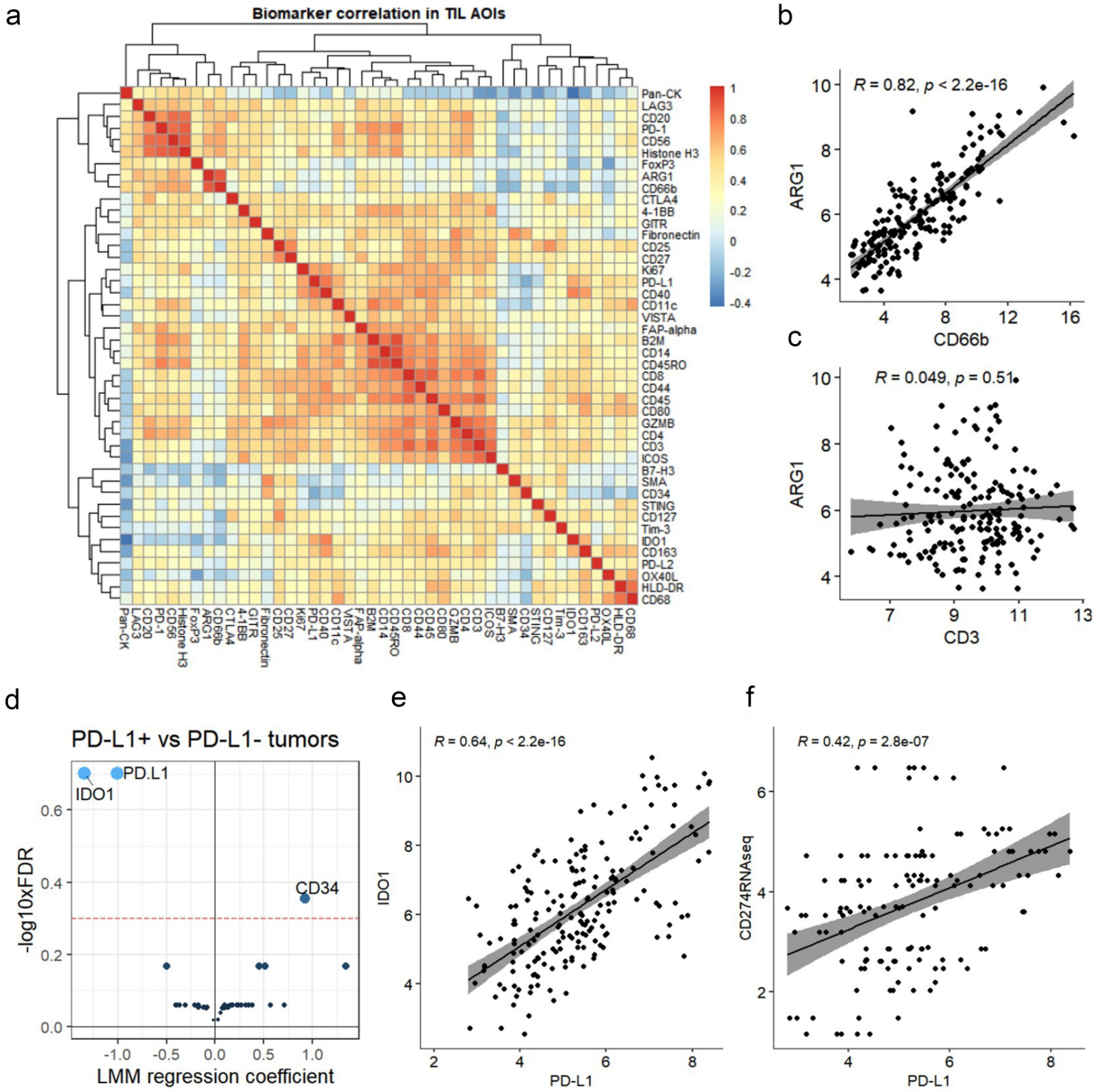

Figure 4. Correlation of potentially targetable markers across areas of illumination (AOIs) and spatial niches. (A) Pearson correlation for TIL AOIs. (B) Correlation of ARG1 to CD66b and (C) ARG1 to CD3 across all AOIs. Pearson R and p-values are shown. (D) Linear Mixed Models (LMM) with Patient ID as random effect for classification of IHC PD-L1 positive versus negative tumors (10% threshold). -log10 false discovery rate (FDR) plotted against LMM regression coefficient with negative coefficient = higher in PD-L1 positive tumors, and vice versa. (E) IDO1 and PD-L1 correlation across all AOIs. (F) PD-L1 (CD274) quantification by bulk RNAseq correlated to DSP PD-L1 as measured in multiple AOIs per patient. Pearson R and p-values are shown.

Correlation of phenotypic and functional antigens suggests OX40L and ARG1 as potential targets in subsets of NSCLC

Correlation analysis confirmed that individual proteins displayed lower variation in TLS, with an overall higher correlation of both abundantly and lowly expressed markers compared to SL and TIL (Supplementary Figure 7). For an increased understanding of interactions driving immune suppression inside tumor nests, clusters of correlating biomarkers were explored in TIL niches (Figure 4A). OX40L and CD68 were in linear mixed models identified as higher expressed in TIL than in SL (Figure 3A). Correlation analysis clustered OX40L and CD68 with HLA-DR, which may indicate that OX40L is primarily expressed by antigen-presenting macrophages in vicinity of tumor cells. A previously identified target, ARG1, was highly correlated to CD66b, both across (Figure 4B) and within spatial immune niches (Supplementary Figure 8). ARG1 and CD66b were poorly correlated with CD3 (Figure 4C) but clustered with FoxP3. Thus, ARG1 may primarily be expressed by CD66b+ granulocytes associated with a CD3-low, immune suppressive environment. The level of CD66b and ARG1 varied significantly between patients (Figure 2C) but did not, in general, differ between stromal and tumor immune niches (Figure 3A).

PD-L1 IHC score and bulk RNAseq were confirmed by DSP and correlate to IDO1

Tumors were grouped as PD-L1 positive and negative based on previously generated IHC scores from the same TMA.[16] Overall, the presence of distinct spatial immune niches was not significantly associated with tumor PD-L1 status, regardless of IHC score threshold (Supplementary Figure 9). PD-L1 ($p = 0.007$) and IDO1 ($p = 0.009$) showed the highest association to PD-L1 IHC-positive tumors, while CD34 was the marker most strongly associated with PD-L1 IHC-negative tumors ($p = 0.030$) (Figure 4D). Similarly, DSP PD-L1 was significantly correlated with bulk RNAseq PD-L1 counts from the same tumors (Figure 4F) and IHC PD-L1 scores (Supplementary Figure 10). Although DSP data obtained from spatially distinct niches are not readily compared to bulk RNA data or overall tumor IHC scores, the positive correlation of markers including PD-L1, CD3, and CD8 (Supplementary Figure 10) points to the validity of the DSP data. The correlation between PD-L1 and IDO1 was high across all AOIs (Figure 4E) and within spatial immune niches (Supplementary Figure 11), however expression levels of the two proteins were significantly higher in TIL compared to SL and TLS (Figure 3A and Supplementary Figure 11). In TIL, IDO1 is clustered with CD163 (Figure 4A), which may suggest that immune suppression conferred by IDO1 is associated with CD163+ macrophages and that combined PD-L1 and IDO1 targeting could be feasible for patients with CD163 presence in the spatial vicinity of tumor cells. Similar to ARG1, which regulates arginine levels critical for lymphocyte proliferation and function, IDO1 is a regulator of tryptophan metabolism. The data indicate that both these markers contribute to immune suppression profiles, suggesting a need to better understand checkpoint-driven mechanisms associated with amino acid metabolism in NSCLC.

Presence of distinct immune infiltration spatial phenotypes or biomarkers was weakly associated to clinical factors and survival

Analysis showed that STING, an activation marker of primarily innate immunity, was positively correlated to tumor stage ($p = 0.054$) (Supplementary Figure 12A) and lymph node status ($p = 0.032$) (Supplementary Figure 12B). The presence of distinct spatial immune niches could not be attributed to patient subgroups based on tumor stage, histology subtype (adenocarcinoma vs. squamous cell carcinoma), gender, or smoking status (Supplementary Figure 12C-F).

Estimated tumor mutational burden was also not associated with immune infiltration profiles, regardless of whether assessing total or non-synonymous mutational load. Individual genes mutated in a minimum of six patients were assessed for impact on the immune microenvironment. KRAS-mutated tumors showed significantly higher expression of CD8, CD3, CD44, CD40, and TIM3 across all AOIs, indicating a more active T-cell response in comparison to wt (Supplementary Figure 13A). Other mutations showing a significant association to immune markers were LRP1B (higher Granzyme B in mutated, Supplementary Figure 13B); KMT2D (lower ICOS, PD-L1, CD80, and VISTA in mutated, Supplementary Figure 13C); and CSMD3 (lower HLA-DR, IDO1, and OX40L in mutated, Supplementary Figure 13D). TP53 mutations were prevalent ($n = 20$, 60%) but showed no significant impact on immune microenvironment compared to wt. EGFR was not tested due to the low number ($n = 3$) of mutated tumors.

Presence of specific immune niches was not correlated to overall or progression-free survival (Supplementary Figure 14A). B7-H3 was the only biomarker demonstrating significance as a predictor of survival (5-year truncated overall survival $p = 0.008$, hazard ratio 0.6) (Supplementary Figure 14B). Of note, established prognostic factors, including tumor stage and patient age, did not show association to survival, indicating that the survival analysis was hampered by the limited number of patient samples.

Discussion

The breakthroughs of immunotherapy and spatially guided tumor analyses of the TIME have jointly provided hope to resolve the biological cues governing response to ICI treatment[17]. To improve outcomes in NSCLC, a better understanding of which patients who will respond to specific immunotherapy, how different therapeutic strategies optimally can be combined, and ways to promote and enhance immune migration and activation in tumors where leukocytes are restricted to stromal areas is warranted. This can only be achieved by taking genetic and phenotypic diversity into account and incorporating methods that can capture and describe complex TIME[18]. In this study, we used DSP[19] to explore the variability of the CD45+ compartment in NSCLC

and to understand how spatially distinct immune infiltration niches differ in cell composition and functional immuno-oncology targets. Through image segmentation, tumor-infiltrating leukocytes (TIL), stromal leukocytes (SL), and tertiary lymphoid structures (TLS) could be compared by DSP protein profiling specifically of CD45+ cells in regions of interest.

TIL areas, defined as having individual immune cells in close contact with tumor cells, were identified in 42% of patients. Importantly, the relative level of lymphocyte phenotypic markers, including CD45, CD3, CD8, and CD3, did not differ between TIL and SL. Instead, the location of immune cells, in either the stroma or tumor cell compartment, was rather associated with distinct functional immune profiles. TIL were surrounded by an environment enriched in IDO1, potentially mediating CD8+ T-cell suppression. The expression of IDO1 is variable in NSCLC.[20]. So far, no IDO1 inhibitor has been approved for cancer treatment but is currently being evaluated in combination with chemo- or radiotherapy[21]. Additionally, several B7 family members/ligands such as CTLA4, B7-H3, PD-L1, and PD-L2 were upregulated in TIL compared to SL. Thus, the properties of distinct immune niches should, rather than the overall level of lymphocytes in the TIME, be considered when strategies to guide the choice of therapy, or to overcome resistance, are developed.

While TIL were generally characterized by immune suppressive phenotypes, CD66b, and ARG1 were observed in TIL and SL immune niches to a similar degree. This indicates that ARG1 targeting may be a feasible approach to break immune suppression also for NSCLC tumors lacking immune infiltration in the immediate tumor vicinity. Given the strong correlation between ARG1 and CD66b observed here, tumors with high granulocyte presence in stroma or tumor regions could potentially be subjected to ARG1 therapy. Concordantly, previous research has demonstrated that increased ARG1 plasma levels are related to IL-8 induced release from neutrophils[22]. ARG1, together with NOS (nitric oxide synthase), controls the level of arginine, which in turn regulates immune activity. In animal experiments, ARG1-directed treatment reduces growth in KRAS-mutated tumors[23]. Neutrophils have been reported to be one of the dominating immune populations in NSCLC[24], and it has recently been shown that high CD66b and TIM-3 protein levels predict poor survival for NSCLC patients, irrespective of mutational status[25].

Over 50% of NSCLC tumors can be characterized as having an excluded TIME phenotype, with most immune cells residing in tumor-adjacent stroma. With less ICI targets present, it is of particular interest to identify alternative approaches to stimulate immune activity in these tumors. Here, we show that CD27 is one of the few functional antigens enriched in the stromal immune niche and that expression increased with distance to tumor cells. CD27 is a member of the tumor necrosis factor receptor superfamily and binds to the checkpoint molecule CD70[26]. The CD27-CD70 axis constitutes an attractive option to stimulate T-cells and augment the effect of ICI[27]. Specifically, CD27 is a potential target for agonistic immunotherapy, using, for example, varlilumab[28] for patients where immune infiltration resides in the stroma rather than in the direct tumor vicinity.

Of interest, T-cells can be recruited to the tumor site through high endothelial venules adjacent to TLS, suggesting that TLS constitute an opportunity to increase T-cell recognition to the tumor[29]. The education of mature dendritic cells in TLS potentially generates a specific immune context characterized by a strong Th1 and cytotoxic orientation associated with favorable outcomes[30,31]. However, the prognostic role of TLS has been debated as other studies have shown that TLS can be dysfunctional and promote the production of regulatory T-cells[7]. It should be noted that the term TLS is only poorly defined and often histologically determined as lymphoid aggregates in HE sections. In this study, we further characterized TLS, here defined as dense stromal leukocyte compartments of high CD45 intensity, on a molecular level, and demonstrate that these lymphoid aggregates are not random cell groups but functional entities with a specific immune repertoire. Even within the limited area of the tissue cores, TLS were identified in 30% of tumors. Phenotypical and functional comparisons to other stromal immune niches showed that TLS were dominated by lymphocytes, including B and T-cells, and the presence of CD11c positive dendritic cells and antigen presentation (HLA-DR, Beta-2-Macroglobulin, and CD40). TLS, compared to SL, were enriched in CTLA4, which indeed indicates that the TLS may be dysfunctional and lack the ability to promote full immunity. Further characterization of these structures, including the level of maturity as marked by, e.g., CD23 expression[32], is needed to elucidate the prognostic impact of the presence and spatial distribution of TLS in NSCLC.

In addition to TIME heterogeneity, analysis of differences in phenotypic and functional immune-related proteins were associated with clinicopathological and genomic features as well as survival. The checkpoint molecule B7-H3 was identified as significantly associated with improved overall survival (5-year truncated), but this finding needs to be validated in a larger cohort. Specific targeting of B7-H3 has shown promising results in a wide range of tumor types[33]. The total mutational burden and most individual genes had no association to immune phenotypes in our limited cohort, but KRAS-mutated cases showed evidence of a tumor-suppressive T-cell environment. A high mutational load should provide a high amount of neoantigens, and previous studies have shown an association to PD-1 treatment sensitivity in NSCLC[34]. Thus, consideration to genetic, proteomic, and spatial contexts combined needs to be made if prognostic indices are to be defined for response to immunotherapy.

Our study was limited by number of patients and restricted to protein profiling of immune compartments, subjectively annotated using 2D images. Single-cell or spatially resolved genomic analysis of larger cohorts, with concomitant spatial profiling of distinct phenotypes, including markers of, e.g., TLS maturity and myeloid subtypes, may reveal which transcriptional programs that are affecting survival and treatment response. By establishing such interactions, it can be pinpointed which biomarkers and spatial features that are relevant to include in an immune index for stratifying patients by tentative therapeutic regimens. As demonstrated here and by others, the DSP technology is valuable for detailed mapping of complex TIME and identification of new targets. Since the

analysis is based on standard FFPE tissue and antibody staining, there is a good opportunity to translate condensed biomarker signatures to the clinical setting, for patient stratification in relation to TIME profiles. Further validation of individual targets shown to be associated with immune infiltration phenotypes in this study will be the subject of follow-up studies.

In summary, we show that spatially guided analyses hold potential for pinpointing which immune-targeting strategies are feasible for NSCLC patients. Our data reveal that leukocytes located in distinct niches, including stroma, tumor-infiltrates, and TLS, show evidence of context-related immune suppression and activity. Of importance, 30% of patients had tumor-infiltrating immune cells with enhanced expression of a variety of checkpoint inhibitors that are targetable with upcoming or already FDA-approved ICIs. For these patients, our data suggest that especially B7-H3, OX40L, and IDO1 carry potential therapeutic values beyond PD-L1 and CTLA-4.

Acknowledgments

The authors wish to acknowledge the support of the staff at the SpatialOmics@LU platform where the experiments were performed.

Disclosure statement

No potential conflict of interest was reported by the authors.

Funding

This work was supported by the Cancera foundation; Lund University Faculty of Engineering; Lund University Faculty of Medicine; Lund University Cancer Center; and the Crafoord Foundation under Grant 20220005.

ORCID

Anna Sandström Gerdtsson http://orcid.org/0000-0003-1932-0365

References

1. Siegel RL, Miller KD, Fuchs HE, Jemal A. Cancer statistics, 2022. CA Cancer J Clin. 2022;72(1):7–33. doi:10.3322/caac.21708.
2. Ramalingam SS, Vansteenkiste J, Planchard D, Cho BC, Gray JE, Ohe Y, Zhou C, Reungwetwattana T, Cheng Y, Chewaskulyong B, et al. Overall survival with osimertinib in untreated, EGFR-Mutated advanced NSCLC. N Engl J Med. 2020;382(1):41–50. doi:10.1056/NEJMoa1913662.
3. Camidge DR, Dziadziuszko R, Peters S, Mok T, Noe J, Nowicka M, Gadgeel SM, Cheema P, Pavlakis N, de Marinis F, et al. Updated efficacy and safety data and impact of the EML4-ALK fusion variant on the efficacy of alectinib in untreated ALK-Positive advanced non–small cell lung cancer in the global Phase III ALEX study. J Thorac Oncol. 2019;14(7):1233–1243. doi:10.1016/j.jtho.2019.03.007.
4. Liu L, Bai H, Wang C, Seery S, Wang Z, Duan J, Li S, Xue P, Wang G, Sun Y, et al. Efficacy and Safety Of First-Line Immunotherapy Combinations For Advanced NSCLC: a systematic review and network meta-analysis. J Thorac Oncol. 2021;16(7):1099–1117. doi:10.1016/j.jtho.2021.03.016.
5. Borghaei H, Paz-Ares L, Horn L, Spigel DR, Steins M, Ready NE, Chow LQ, Vokes EE, Felip E, Holgado E, et al. Nivolumab versus docetaxel in advanced nonsquamous non–small-cell lung cancer. N Engl J Med. 2015;373(17):1627–1639. doi:10.1056/NEJMoa1507643.
6. Genova C, Dellepiane C, Carrega P, Sommariva S, Ferlazzo G, Pronzato P, Gangemi R, Filaci G, Coco S, Croce M. Therapeutic implications of tumor microenvironment in lung cancer: focus on immune checkpoint blockade. Front Immunol. 2021;12:799455. doi:10.3389/fimmu.2021.799455.
7. Altorki NK, Markowitz GJ, Gao D, Port JL, Saxena A, Stiles B, McGraw T, Mittal V. The lung microenvironment: an important regulator of tumour growth and metastasis. Nat Rev Cancer. 2019;19(1):9–31. doi:10.1038/s41568-018-0081-9.
8. Zugazagoitia J, Gupta S, Liu Y, Fuhrman K, Gettinger S, Herbst RS, Schalper KA, Rimm DL. Biomarkers associated with beneficial PD-1 checkpoint blockade in non–small cell lung cancer (NSCLC) identified using high-plex digital spatial profiling. Clin Cancer Res. 2020;26(16):4360–4368. doi:10.1158/1078-0432.CCR-20-0175.
9. Allam M, Hu T, Lee J, Aldrich J, Badve SS, Gokmen-Polar Y, Bhave M, Ramalingam SS, Schneider F, Coskun AF. Spatially variant immune infiltration scoring in human cancer tissues. NPJ Precis Oncol. 2022;6(1):60. doi:10.1038/s41698-022-00305-4.
10. Wu F, Fan J, He Y, Xiong A, Yu J, Li Y, Zhang Y, Zhao W, Zhou F, Li W, et al. Single-cell profiling of tumor heterogeneity and the microenvironment in advanced non-small cell lung cancer. Nat Commun. 2021;12(1):2540. doi:10.1038/s41467-021-22801-0.
11. Lewis SM, Asselin-Labat ML, Nguyen Q, Berthelet J, Tan X, Wimmer VC, Merino D, Rogers KL, Naik SH. Spatial omics and multiplexed imaging to explore cancer biology. Nat Methods. 2021;18(9):997–1012. doi:10.1038/s41592-021-01203-6.
12. Brunnstrom H, Johansson A, Westbom-Fremer S, Backman M, Djureinovic D, Patthey A, Isaksson-Mettävainio M, Gulyas M, Micke P. PD-L1 immunohistochemistry in clinical diagnostics of lung cancer: inter-pathologist variability is higher than assay variability. Mod Pathol. 2017;30(10):1411–1421. doi:10.1038/modpathol.2017.59.
13. La Fleur L, Falk-Sorqvist E, Smeds P, Berglund A, Sundstrom M, Mattsson JS, Brandén E, Koyi H, Isaksson J, Brunnström H, et al. Mutation patterns in a population-based non-small cell lung cancer cohort and prognostic impact of concomitant mutations in KRAS and TP53 or STK11. Lung Cancer. 2019;130:50–58. doi:10.1016/j.lungcan.2019.01.003.
14. Djureinovic D, Hallstrom BM, Horie M, Mattsson JSM, La Fleur L, Fagerberg L, Brunnström H, Lindskog C, Madjar K, Rahnenführer J, et al. Profiling cancer testis antigens in non–small-cell lung cancer. JCI Insight. 2016;1(10):e86837. doi:10.1172/jci.insight.86837.
15. Beechem JM. High-Plex spatially resolved RNA and protein detection using digital spatial profiling: a technology designed for immuno-oncology biomarker discovery and translational research. Methods Mol Biol. 2020;2055:563–583.
16. Backman M, La Fleur L, Kurppa P, Djureinovic D, Elfving H, Brunnstrom H, Mattsson JSM, Lindberg A, Pontén V, Eltahir M, et al. Infiltration of NK and plasma cells is associated with a distinct immune subset in non-small cell lung cancer. J Pathol. 2021;255(3):243–256. doi:10.1002/path.5772.
17. Rad HS, Rad HS, Shiravand Y, Radfar P, Arpon D, Warkiani ME, O'Byrne K, Kulasinghe A. The Pandora's box of novel technologies that may revolutionize lung cancer. Lung Cancer. 2021;159:34–41. doi:10.1016/j.lungcan.2021.06.022.
18. Hanahan D, Coussens LM. Accessories to the crime: functions of cells recruited to the tumor microenvironment. Cancer Cell. 2012;21(3):309–322. doi:10.1016/j.ccr.2012.02.022.
19. Merritt CR, Ong GT, Church SE, Barker K, Danaher P, Geiss G, Hoang M, Jung J, Liang Y, McKay-Fleisch J, et al. Multiplex digital spatial profiling of proteins and RNA in fixed tissue. Nat Biotechnol. 2020;38(5):586–599. doi:10.1038/s41587-020-0472-9.
20. Zhang ML, Kem M, Mooradian MJ, Eliane JP, Huynh TG, Iafrate AJ, Gainor JF, Mino-Kenudson M. Differential expression

of PD-L1 and IDO1 in association with the immune microenvironment in resected lung adenocarcinomas. Mod Pathol. 2019;32(4):511–523. doi:10.1038/s41379-018-0160-1.
21. Ladomersky E, Zhai L, Lenzen A, Lauing KL, Qian J, Scholtens DM, Gritsina G, Sun X, Liu Y, Yu F, et al. IDO1 inhibition synergizes with radiation and PD-1 blockade to durably increase survival against advanced glioblastoma. Clin Cancer Res. 2018;24(11):2559–2573. doi:10.1158/1078-0432.CCR-17-3573.
22. Rotondo R, Barisione G, Mastracci L, Grossi F, Orengo AM, Costa R, Truini M, Fabbi M, Ferrini S, Barbieri O. IL-8 induces exocytosis of arginase 1 by neutrophil polymorphonuclears in nonsmall cell lung cancer. Int J Cancer. 2009;125(4):887–893. doi:10.1002/ijc.24448.
23. Miret JJ, Kirschmeier P, Koyama S, Zhu M, Li YY, Naito Y, Wu M, Malladi VS, Huang W, Walker W, et al. Suppression Of myeloid cell arginase activity leads to therapeutic response in a NSCLC mouse model by activating anti-tumor immunity. J ImmunoTher Cancer. 2019;7(1):32. doi:10.1186/s40425-019-0504-5.
24. Kargl J, Busch SE, Yang GH, Kim KH, Hanke ML, Metz HE, Hubbard JJ, Lee SM, Madtes DK, McIntosh MW, et al. Neutrophils dominate the immune cell composition in non-small cell lung cancer. Nat Commun. 2017;8:14381. doi:10.1038/ncomms14381.
25. Shen M, Jiang K, Sui Y, Xu Z, Cui H, Wang Y, Zhang H, Xu Z, Xu W, Ding Q, et al. Characterization of CD66b and its relationship between immune checkpoints and their synergistic impact in the prognosis of surgically resected lung adenocarcinoma. Lung Cancer. 2021;160:84–91. doi:10.1016/j.lungcan.2021.08.012.
26. Flieswasser T, Van den Eynde A, Van Audenaerde J, De Waele J, Lardon F, Riether C, de Haard H, Smits E, Pauwels P, Jacobs J. The CD70-CD27 axis in oncology: the new kids on the block. J Exp Clin Cancer Res. 2022;41(1):12. doi:10.1186/s13046-021-02215-y.
27. Lutfi F, Wu L, Sunshine S, Cao X. Targeting the CD27-CD70 pathway to improve outcomes in both checkpoint immunotherapy and allogeneic hematopoietic cell transplantation. Front Immunol. 2021;12:715909. doi:10.3389/fimmu.2021.715909.
28. Starzer AM, Berghoff AS. New emerging targets in cancer immunotherapy: cD27 (TNFRSF7). ESMO Open. 2020;4(Suppl 3):e000629. doi:10.1136/esmoopen-2019-000629.
29. de Chaisemartin L, Goc J, Damotte D, Validire P, Magdeleinat P, Alifano M, de Chaisemartin L, Cremer I, Fridman W-H, Sautès-Fridman C, et al. Characterization of chemokines and adhesion molecules associated with T cell presence in tertiary lymphoid structures in human lung cancer. Cancer Res. 2011;71(20):6391–6399. doi:10.1158/0008-5472.CAN-11-0952.
30. Germain C, Gnjatic S, Tamzalit F, Knockaert S, Remark R, Goc J, Lepelley A, Becht E, Katsahian S, Bizouard G, et al. Presence of B cells in tertiary lymphoid structures is associated with a protective immunity in patients with lung cancer. Am J Respir Crit Care Med. 2014;189(7):832–844. doi:10.1164/rccm.201309-1611OC.
31. Goc J, Germain C, Vo-Bourgais TK, Lupo A, Klein C, Knockaert S, de Chaisemartin L, Ouakrim H, Becht E, Alifano M, et al. Dendritic cells in tumor-associated tertiary lymphoid structures signal a Th1 cytotoxic immune contexture and license the positive prognostic value of infiltrating CD8+ T cells. Cancer Res. 2014;74(3):705–715. doi:10.1158/0008-5472.CAN-13-1342.
32. Vanhersecke L, Brunet M, Guegan JP, Rey C, Bougouin A, Cousin S, Le Moulec S, Besse B, Loriot Y, Larroquette M, et al. Mature tertiary lymphoid structures predict immune checkpoint inhibitor efficacy in solid tumors independently of PD-L1 expression. Nat Cancer. 2021;2(8):794–802. doi:10.1038/s43018-021-00232-6.
33. Kontos F, Michelakos T, Kurokawa T, Sadagopan A, Schwab JH, Ferrone CR, Ferrone S. B7-H3: an attractive target for antibody-based immunotherapy. Clin Cancer Res. 2021;27(5):1227–1235. doi:10.1158/1078-0432.CCR-20-2584.
34. Rizvi NA, Hellmann MD, Snyder A, Kvistborg P, Makarov V, Havel JJ, Lee W, Yuan J, Wong P, Ho TS, et al. Mutational landscape determines sensitivity to PD-1 blockade in non–small cell lung cancer. Science. 2015;348(6230):124–128. doi:10.1126/science.aaa1348.